

## GROUND CONTROL POINTS AND THEIR INFLUENCES ON THE PRECISION OF GENERATING A DIGITAL SURFACE MODEL USING AN UNMANNED AERIAL VEHICLE

**Purpose.** To determine the optimal number and spatial distribution of Ground Control Points (GCPs) required to achieve high-precision georeferencing in unmanned aerial vehicle (UAV) imagery, particularly for applications requiring 1:1,000 scale mapping.

**Methodology.** Seven experimental scenarios were conducted, varying the number of GCPs from 4 to 30. For each scenario, GCPs were arranged in seven different spatial configurations, including central, corner, edge, and evenly distributed placements. The Root Mean Squared Error (RMSE) was calculated for each configuration to assess georeferencing accuracy.

**Findings.** The results showed that using only 4 GCPs produced the highest RMSE, indicating the lowest accuracy. RMSE values decreased as the number of GCPs increased, with minimal improvement beyond 20 GCPs. Among all distribution patterns, placing GCPs at the corners consistently resulted in the highest RMSE. The most accurate results were achieved with 20 evenly distributed GCPs.

**Originality.** This study provides a systematic evaluation of both the quantity and spatial arrangement of GCPs in UAV photogrammetry, offering empirical evidence to support optimal GCP deployment strategies.

**Practical value.** The findings offer practical guidance for UAV mapping professionals, suggesting that 20 evenly distributed GCPs are sufficient to meet the accuracy standards for 1:1,000 scale maps. This helps optimize fieldwork efficiency while ensuring data quality.

**Keywords:** *ground control points, Digital Surface Model, unmanned aerial vehicle*

**Introduction.** Nowadays, instead of using traditional methods, many industries have used advanced technology such as unmanned aerial vehicles (UAVs) or drones for gathering, analyzing, and proceeding data of interest [1]. In the mining industry, mining operations are usually performed in isolated and difficult-to-access areas. As a result, decision-making is delayed, and the obtained data is insufficient. UAVs provide speedy, safe, and affordable aerial surveys for data collection. This is especially helpful for industries like mining, which need continuous monitoring [2]. UAV technology can be widely used in mining activities, such as topographical surveying and mapping [3], monitoring of ground subsidence and horizontal displacements [4], analyzing slope stability [5], detecting erosion [6], monitoring mine waste dump [7], creating a system for automatically controlling of UAV movement in a mine's restricted area [8], etc.

The majority of the aforementioned applications require a high-accuracy Digital Surface Model (DSM). Although there are different approaches used to produce DSM with high precision such as terrestrial laser scanning systems, Airborne Light Detection and Ranging (LiDAR) [9], satellite images [10], aerial photogrammetry [11]; UAV photogrammetry is one of the most effective methods because it integrates the strengths of airborne and close-range photogrammetry [12]. In comparison with aerial photogrammetry, it ensures cheaper data gathering and takes less time. In addition, the combination of UAV photogrammetry and computer systems yields data that is more precise [13]. Therefore, the creation of UAV-based DSM in mining areas and the assessment of its accuracy can be identified in many studies [14]. It is difficult to assess the quality of

UAV-based photogrammetric products including DSM because there are a lot of factors that need to be considered, such as the focal length of the camera [15], flight altitude and orientation parameters [16], image quality [17], dedicated software, image resolution, Unmanned Aerial System (UAS) system configuration, ground sample distance [18], the number of ground control point and their distribution, etc. Among all the parameters mentioned above, the number and distribution of the GCPs are the criteria with the greatest impact on the precision of the DSM [19]. Identifying the suitable number of ground control points and their arrangement is one of the most time-consuming works [12]. Although it takes a lot of time, the GCPs can significantly improve the precision of the three-dimensional (3D) data and their determination is a crucial step in georeferencing the UAV photo blocks. Furthermore, if a sub-decimeter accuracy in elevation is required, the GCPs have to be considered in the project design [20].

In recent years, researchers have been particularly interested in determining the optimal number of GCPs required for a UAV flight. Several studies have been carried out to assess the precision of products derived from UAV photos by altering the quantity and distribution of GCPs [21]. Most studies have shown that, to improve the accuracy of DSM generation, GCPs should be evenly distributed around the study area, and the more the number of GCPs utilized, the higher the overall precision [20, 22]. However, among the previous research, there have not been many studies applied in mining areas and the number of publications is very limited for mining locations with complex terrain, small and medium scales. According to [23], in open-pit mines, UAV technology is used to generate DSM, and it is proven that the more GCPs there are, the more precise the

DSM will be. Therefore, to choose their appropriate number and network configuration in the Long Son quarry, they conducted the analysis of DSMs created using 8 scenarios with 18 GCPs and five different network forms for each case. Experiments indicated that a higher number of GCPs improves DSM accuracy and reduces reliance on the GCPs' network configuration. Similarly, in order to evaluate the precision of DSM of an open pit mine using UAV images and the Structure from motion (SfM) method, [24] tested 13 scenarios with 177 GCPs and proposed to distribute 18 to 20 GCPs uniformly throughout each image block to obtain the best results. In addition, [25] has determined the optimal configuration of GCPs to ensure the accuracy of DSM in quarry sites. The obtained findings revealed that the uniformly distributed GCP set is the optimal configuration, and the more GCPs with an even distribution that are employed, the more accurate the SfM-based DSM is. Also, [26] performed numerous experiments to evaluate the influence of GCPs' distribution on 3D model precision and identify the minimum number of GCPs that can be used in open-pit gravel mines. They found that DSMs constructed with fewer GCPs had lower accuracy than DSMs constructed with more GCPs. At the same time, a system of evenly distributed GCPs produced better quality DSMs than the others.

When using UAVs to build digital surface models of open-pit mine shore areas, Dieu, et.al (2017) realized that the accuracy of DEMs and DSMs changed when the geometry and number of GCPs varied. This conclusion was also confirmed by Long, et al. (2021) when studying open-pit mines using UAV photography. The results showed that the accuracy of DSM improved when the number of GCPs increased, and the authors also proposed that the number of GCPs was sufficient to achieve an overall accuracy of less than 10 cm for small and medium-sized open-pit mines with an area of about 36 hectares. In another study, the authors evaluated the usability of the low-cost Phantom 4 Pro drone to build DSM and map at 4 quarries with different terrain characteristics. The results of this study show that when the number of control points is evenly distributed on the mine surface and the flight height is reasonable, the accuracy in both the ground and height is sufficient to ensure the establishment of large-scale maps [27].

Thus, the influence of the number of GCPs and their distribution on the results of DSM formation from UAV images has been demonstrated in several studies. However, the number of relevant publications is still relatively limited for mineral mining areas with complex terrain and small areas. Therefore, this study was conducted to analyze and confirm the influence of the above factors on the accuracy of DSMs generated from UAV images for areas with complicated topography, significant elevation differences, and limited areas.

**Study area.** The study area is a mining and processing site managed by Tan Tien Co., Ltd., located in Yen Bai Province in the Northwest-Northeast region of Vietnam (Fig. 1).

The experimental site covers approximately 19.1 ha and is characterized by heterogeneous terrain and relatively high elevation variation across a small area. According to the Digital Elevation Model (Fig. 2), ground elevation within the study area ranges from 77 to 163 m



Fig. 1. The study area

above sea level, yielding a vertical relief of about 86 m. Such a difference in elevation across a limited spatial extent results in a complex topography, including steep slopes, benches, quarry pits, stockpiles, and fragmented vegetation patches. Fig. 2 (DEM of the study area) clearly illustrates the uneven distribution of elevation: higher zones appear as small peaks and benches interspersed with local depressions and drainage channels. Elevation changes are not only lateral but also abrupt along quarry boundaries and slope cuts.

This heterogeneity is highlighted in the cross-sectional profiles presented in Figs. 3 and 4. Both profiles demonstrate alternating steep segments (with sharp elevation gains or drops over short distances) and nearly flat sections, forming a discontinuous landform structure typical of active mining areas subjected to excavation, leveling, and dumping activities.

Surface cover in the study area is diverse. Exposed soil, bare rock, mud, and stockpiled mining material dominate, interspersed with secondary vegetation patches. This patchy cover generates strong spectral and textural contrasts in UAV imagery, posing challenges for feature detection and image matching during dense point cloud generation. In addition, artificial structures such as quarry benches, stockyards, and internal roads introduce sharp edges and abrupt slope changes, which may reduce the consistency of tie-point extraction in

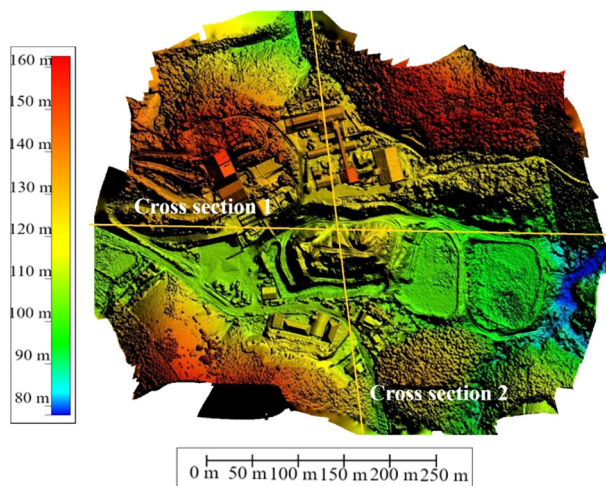


Fig. 2. DEM of study area

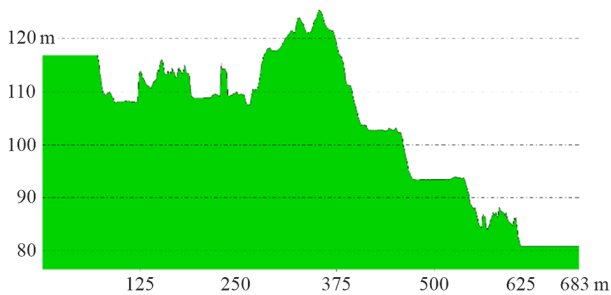


Fig. 3. Terrain changes in cross-section direction 1

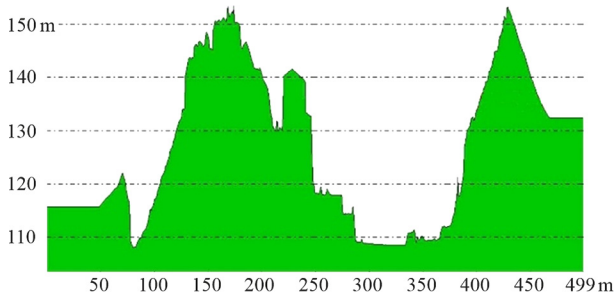


Fig. 4. Terrain changes in cross-section direction 2

Structure-from-Motion (SfM) workflows. These topographic characteristics have two important implications for UAV surveys and the production of high-quality DSMs. First, the vertical relief of ~86 m across a compact area increases the need for a sufficient number and careful spatial distribution of Ground Control Points to ensure accurate camera calibration and to minimize elevation errors. Rapid slope changes also require GCPs to be placed across both high and low areas as well as along quarry edges to adequately capture landform variations. Second, the fragmented surface structure (bare ground, vegetation, mineral piles) necessitates careful flight planning and camera parameter settings (e.g., high forward and side overlap, appropriate flying altitude) to reduce occlusion and increase the number of homologous points between overlapping images.

Selecting this experimental site in Yen Bai Province provides high representativeness for UAV-based studies in small- to medium-scale mining environments. The area contains both anthropogenic landforms (quarry benches, drainage ditches, waste piles) and natural topographic features (slopes, depressions), making it particularly suitable for analyzing the influence of GCP number and distribution on DSM accuracy.

The study area, despite its relatively small extent, exhibits highly heterogeneous terrain with considerable elevation relief and complex surface cover. This environment provides an ideal testbed for evaluating the impact of GCP quantity and spatial distribution on DSM accuracy. Observations from Figs. 1–4 confirm the necessity of adopting rational GCP placement strategies (covering edges, corners, and central zones) and form the practical basis for the experimental scenarios described in the subsequent sections of this paper.

**Materials and methods.** The methodology used to evaluate the precision of UAV based on the number of control points and their distribution is shown in Fig. 5 including two primary stages.

The fieldwork, which included setting up the GCPs and CPs on the land, taking the measurements, and

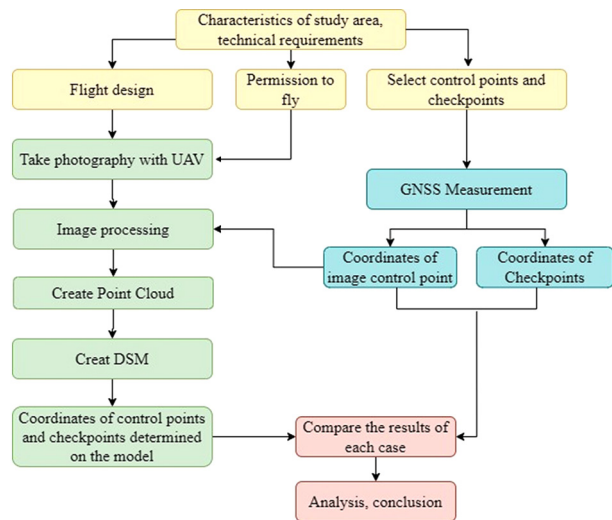


Fig. 5. Processing change of completing the work

conducting flight operations, is the first phase. Next, the office work involved transferring the flight photographs to a computer, data processing using photogrammetric software, and creating point clouds, orthophoto maps, and DSMs.

**Data collection.** Determination of the image control points. Before conducting the flight, it is necessary to select image control points, some of which are used to build the DSM model, and the remaining points are used to evaluate the accuracy of the DSM model. The number of control points in the research area includes 62 control points situated evenly throughout the study area. Fig. 6 is an example of a selected control point in the study area. Those points are measured to 02 national coordinate origin points in the VN2000 coordinate system. However, after checking, 01 point did not meet the required accuracy, so it was removed and there were only 61 GCPs points left (used for image correction and check). The study used a Real Time Kinematic (RTK) ComNav T300 receiver and the static measurement method to measure the image control network. The control points were marked with highly reflective materials to increase contrast.

**UAV and camera.** The experimental data were collected using a GNSS device and a DJI Inspire 2 UAV. The main components mounted on the fuselage include four motors, four removable propellers, a 5-way collision avoidance sensor, and fixed landing legs underneath. In addition, the UAV is controlled by buttons on



Fig. 6. Ground control point markers

Technical specifications of instruments used in the study

DJI Inspire 2				Camera				
Weight, g	Maximum speed, miles/hour	Maximum flight time, min	Antenna frequency, GHz	Camera model	Resolution	Focal length, mm	Pixel size, $\mu\text{m}$	Precalibrated
4,250	58	27	2.4 and 5.8	FC6510 (8.8 mm)	5,472 × 3,648	8.8	2.41 × 2.41	No

a remote controller that has two integrated antennas and a port to connect to a tablet or smartphone, allowing for setting parameters for taking photos or directly displaying images from the UAV. The UAV technical specifications used in this study are shown in Table 1.

**Data collection.** The study used the specialized software Map Pilot to design flight routes integrated with Google map background. The flight process was conducted in safe mode, so the UAV could automatically move according to the designed program. The parameters related to the flight process were calculated to suit the research terrain, with 10 flight bands, image coverage of 75–80 %, flight altitude of approximately 100 m, and flight speed of approximately 5 m/s. In addition, the UAV system and the space around the take-off and landing locations such as high-rise buildings, power lines, trees, antenna poles, transmission stations, etc. were checked before the flight to ensure safety and to obtain the best GNSS signals. The flight was carried out by maintaining the aircraft's altitude throughout the flight. As a result, a total of 411 images were taken covering an area of 19.1 ha, these images were used to build the DSM.

**Methodology. Data preparation.** To analyze the influence of the number of GCPs on the accuracy of DSM, 7 cases were designed with the number of GCPs being 4, 5, 10, 15, 20, 25 points and the CPs being 57, 56, 51, 46, 41, 36, 31 as shown in Table 2.

After determining the appropriate number of GCPs, their distribution is examined to assess the influence of these points on the quality of the resulting DSM. The study selected GCPs at different locations, such as concentrated in the center, upper left corner, upper right corner, lower left corner, lower right corner, evenly distributed, and at the edge of the study area as shown in Fig. 7.

**Data processing.** This study uses the Agisoft Metashape Professional software version 1.5.2 Build 7838 (64-bit) to perform image matching, point cloud generation, DSM construction, and image map establishment. This software with Multi-View 3D reconstruction technology is one of the useful solutions in creating high quality 3D images from static images, working effectively in both controlled and uncontrolled conditions. The image alignment and 3D model reconstruction processes are fully automated in this software [28]. There are two primary phases to the image process including block orientation and DSM generation. The primary aim of this study is to assess how the number of GCPs affects the accuracy of DSM. Therefore, all processing parameters remain consistent. The quality of creating dense clouds and the precision of photo alignment accuracy were both assigned a medium [23]. There are four steps in the SfM processing: 1) image alignment; 2) optimizing alignment including correcting for a rolling shutter; 3) generating a dense cloud relying on

Table 2

Number of GCPs and CPs used for different cases

Case	Number of GCPs	Name of GCPs	Number of CPs	Name of CPs
1	4	7, 30, 40, 53	57	2-3-4-5-6-8-9-10-11-12-13-14-15-16-17-18-19-20-21-22-23-24-25-26-27-28-29-31-32-33-34-35-36-37-38-39-41-42-43-44-45-46-47-48-50-51-52-54-55-56-57-58-59-60-61-62-63
2	5	7, 18, 30, 36, 40	56	2-3-4-5-6-8-9-10-11-12-13-14-15-16-17-19-20-21-22-23-24-25-26-27-28-29-31-32-33-34-35-37-38-39-41-42-43-44-45-46-47-48-50-51-52-53-54-55-56-57-58-59-60-61-62-63
3	10	3, 7, 12, 18, 30, 36, 38, 40, 43, 59	51	2-4-5-6-8-9-10-11-13-14-15-16-17-19-20-21-22-23-24-25-26-27-28-29-31-32-33-34-35-37-39-41-42-44-45-46-47-48-50-51-52-53-54-55-56-57-58-60-61-62-63
4	15	3, 7, 12, 18, 30, 36, 38, 40, 43, 59	46	2-4-5-6-8-9-10-11-13-14-15-16-17-19-20-21-22-23-24-25-26-27-28-29-31-32-33-34-35-37-39-41-42-44-45-46-47-48-50-51-52-53-54-55-56-57-58-60-61-62-63
5	20	2, 10, 13, 16, 17, 18, 20, 21, 23, 30, 35, 37, 40, 42, 45, 47, 48, 52, 56, 59	41	2-3-4-5-6-7-8-9-10-11-12-13-14-15-16-17-18-19-20-21-22-23-24-25-26-27-28-29-30-31-32-33-34-35-36-37-38-39-40-41-42-43-44-45-46-47-48-50-51-52-53-54-55-56-57-58-59-60-61-62-63
6	25	2, 10, 13, 15, 16, 17, 18, 20, 21, 22, 23, 25, 30, 31, 35, 37, 38, 40, 42, 45, 47, 48, 52, 56, 59	36	3-4-5-6-7-8-9-11-12-14-19-24-26-27-28-29-32-33-34-36-39-41-43-44-46-50-51-53-54-55-57-58-60-61-62-63
7	30	2, 6, 10, 13, 15, 16, 17, 18, 19, 20, 21, 22, 23, 25, 28, 30, 31, 35, 37, 38, 40, 42, 45, 46, 47, 48, 51, 52, 56, 59	31	3-4-5-7-8-9-11-12-14-24-26-27-29-32-33-34-36-39-41-43-44-50-53-54-55-57-58-60-61-62-63

Standards for positional error of a point on topographic maps

Scale	$RMSE_{XY}$ , cm	$RMSE_Z$ , cm
1:1,000	≤ 10.0	≤ 25.0

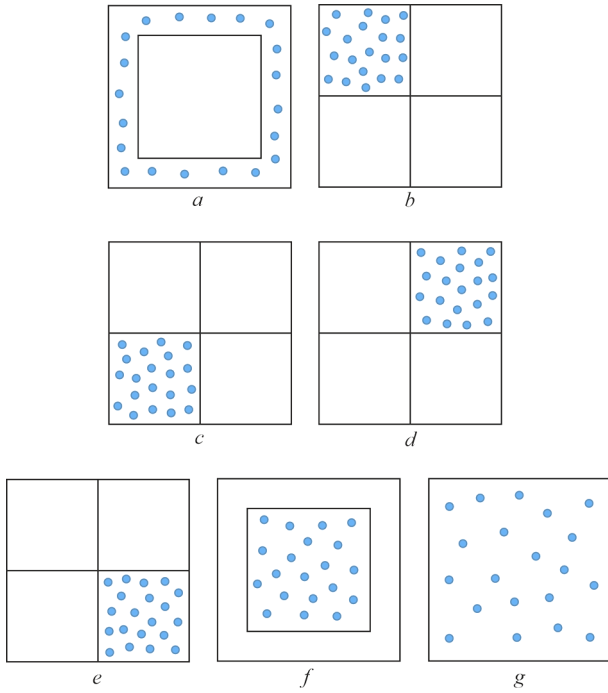


Fig. 7. Distribution of image control points in the area:  
*a* – edge; *b* – upper left corner; *c* – lower left corner; *d* – upper right corner; *e* – lower right corner; *f* – center; *g* – entire study area

medium quality and disabling depth filtering; 4) exporting point coordinates along with their normal and colors from the dense cloud in TXT file.

**Accuracy assessment.** This is a necessary and important step when establishing DSM from UAV images. In this study, the accuracy of DSM is evaluated by comparing the control points on the DSM model with the corresponding points on the ground (the coordinates of these points are determined by the GNSS method). These points are not incorporated in the image processing and their coordinates and altitude have been determined. The following formulas are used to assess the accuracy of DSM

$$\Delta X_i = X_{DSMi} - X_{GSNNi};$$

$$\Delta Y_i = Y_{DSMi} - Y_{GSNNi};$$

$$\Delta Z_i = Z_{DSMi} - Z_{GSNNi};$$

$$RMSE_X = \sqrt{\left[ \left( \frac{1}{n} \right) \sum_{i=1}^n \Delta X_i^2 \right]};$$

$$RMSE_Y = \sqrt{\left[ \left( \frac{1}{n} \right) \sum_{i=1}^n \Delta Y_i^2 \right]};$$

$$RMSE_Z = \sqrt{\left[ \left( \frac{1}{n} \right) \sum_{i=1}^n \Delta Z_i^2 \right]};$$

$$RMSE_{XY} = \sqrt{\left[ \left( \frac{1}{n} \right) \sum_{i=1}^n [\Delta X_i^2 + \Delta Y_i^2] \right]};$$

$$RMSE_{XYZ} = \sqrt{\left[ \left( \frac{1}{n} \right) \sum_{i=1}^n [\Delta X_i^2 + \Delta Y_i^2 + \Delta Z_i^2] \right]},$$

where  $(X_{GSNNi}, Y_{GSNNi}, Z_{GSNNi})$  and  $(X_{DSMi}, Y_{DSMi}, Z_{DSMi})$  are the 3D coordinates of the  $i^{th}$  CP that were acquired

utilizing GNSS survey, and corresponding coordinates on the creating DSM, respectively;  $\Delta X_i, \Delta Y_i, \Delta Z_i$  are coordinate component difference values;  $RMSE_X, RMSE_Y, RMSE_{XY}$  are Root Mean Square Error in the horizontal;  $MSE_Z$  is Root Mean Square Error in the vertical;  $RMSE_{XYZ}$  is Root Mean Square Error in the horizontal and the vertical;  $n$  is the number of the CPs

The obtained RMSE needs to meet the requirements of the standard for establishing a 1:1,000 scale map in the mining area. Table 3 displays the regulations for position error of points on topographic maps at a scale of 1:1,000 [29].

**Results and discussion.** From the errors obtained in each case, using the formulas from (1–8), the RMSE in the horizontal, the vertical, and the total error of the corresponding image control points and checkpoints will be determined. The detailed errors are shown in Tables 4 and 5.

The obtained results show that the number of GCPs and CPs significantly affects the RMSE of GCPs and CPs as well as the accuracy of DSM. On an area of 19.1 ha of complex terrain with large elevation differences like the research area, when the number of GCPs increases (CPs decrease), their errors in the vertical, horizontal, and combined errors decrease, indicating the accuracy of DSM will increase. The analysis of Table 3 revealed that the highest RMSEs occurred in the study area with 4 GCPs, whereas the smallest values were observed with 30 GCPs. When four GCPs were used, their highest RMSE was 9.9 cm in the vertical, 14.8 cm in the horizontal, and 17.9 cm (the total), respectively. Accordingly, the errors of the CPs are also the largest in this case, with 20.3 cm for altitude, 15.8 cm for horizontal, and 25.9 cm for total. Thus, if only four GCPs are used to generate DSM, the RMSE of the GCPs and CPs obtained is 14.8 and 15.8 cm, respectively, which does not meet the accuracy standard for establishing 1:1,000 scale maps for mining projects as specified in Table 2. However, with the addition of just one GCP, the error of those points is significantly improved, reducing from 9.9 cm (RMSE<sub>Z</sub>), 14.8 cm (RMSE<sub>XY</sub>), and 17.9 cm (RMSE<sub>XYZ</sub>) in the case of 4 points to 9.0, 8.4, and 12.4 cm for the 5-point case, respectively. In particular, the RMSE obtained in the case of 5 GCPs shows that this number of points fully meets the accuracy requirements for creating a DSM for mapping in mineral exploitation areas at a scale of 1:1,000.

Additionally, the obtained results also show that the RMSEs decrease as the number of GCPs increases to 10, 15, 20, 25, and 30 points (Fig. 8). This means that, when establishing DSM from UAV images in the study area, except for the first case using 4 GCPs giving large RMSE results, all the remaining 6 options give results with the required accuracy. However, the RMSEs of these GCPs did not change much in the cases using 20, 25, and 30 points (Fig. 8) ( $RMSE_z$ : 5.8–6.0 cm;  $RMSE_{xy}$ : 5.8–5.9 cm; and  $RMSE_{xyz}$ : 8.2–8.4 cm). Even for CPs

Table 4

RMSEs of GCPs for 7 cases

Number of GCPs	Cases	$RMSE_z$	$RMSE_{xy}$	$RMSE_{xyz}$	Number of GCPs	Cases	$RMSE_z$	$RMSE_{xy}$	$RMSE_{xyz}$
4	4_1	7.3	14.6	16.3	20	20_1	5.9	5.7	8.2
	4_2	11.0	15.1	18.6		20_2	6.4	6.3	9.0
	4_3	12.4	14.8	19.3		20_3	6.6	6.3	9.1
	4_4	12.6	14.9	19.5		20_4	6.3	6.4	9.0
	4_5	11.5	15.0	18.9		20_5	6.5	6.4	9.1
	4_6	8.5	14.2	16.5		20_6	6.6	6.0	8.9
	4_7	6.1	14.0	15.2		20_7	3.9	4.2	5.7
	Average	9.9	14.8	17.9		Average	6.0	5.9	8.4
5	5_1	7.7	8.1	11.2	25	25_1	5.9	5.6	8.1
	5_2	10.6	8.6	13.6		25_2	6.2	6.4	8.9
	5_3	10.9	8.5	13.9		25_3	6.2	6.3	8.8
	5_4	10.5	8.7	13.7		25_4	6.5	6.4	9.1
	5_5	10.2	8.9	13.5		25_5	6.3	6.3	8.9
	5_6	9.0	8.4	12.3		25_6	6.1	6.0	8.6
	5_7	5.0	7.8	9.3		25_7	3.8	3.8	5.4
	Average	9.0	8.4	12.4		Average	5.8	5.8	8.2
10	10_1	8.1	7.2	10.9	30	30_1	5.5	5.8	8.0
	10_2	8.2	7.8	11.6		30_2	6.8	6.3	9.3
	10_3	8.2	7.9	11.4		30_3	6.8	6.2	9.2
	10_4	8.5	7.8	11.5		30_4	6.1	6.1	8.6
	10_5	8.9	7.7	11.8		30_5	6.3	6.1	8.8
	10_6	8.5	7.4	11.2		30_6	6.2	5.9	8.6
	10_7	4.6	6.8	8.2		30_7	3.9	3.9	5.5
	Average	7.8	7.5	10.9		Average	5.9	5.8	8.3
15	15_1	7.0	6.6	9.6	—	—	—	—	—
	15_2	7.8	7.1	10.5	—	—	—	—	—
	15_3	9.0	6.9	11.3	—	—	—	—	—
	15_4	8.3	7.0	10.9	—	—	—	—	—
	15_5	8.6	6.9	11.1	—	—	—	—	—
	15_6	7.1	6.8	9.8	—	—	—	—	—
	15_7	4.2	6.2	7.5	—	—	—	—	—
	Average	7.4	6.8	10.3	—	—	—	—	—

(Fig. 9), the variation of RMSE is insignificant and fluctuates around  $15.7 \pm 0.1$  cm ( $RMSE_z$ ),  $7.0 \pm 0.1$  cm ( $RMSE_{xy}$ ), and  $17.3 \pm 0.1$  cm ( $RMSE_{xyz}$ ). Therefore, it will be wasteful to increase the number of points too much while the accuracy is not improved, which means that increasing the number of points beyond 20 points is unnecessary. Therefore, for the study area of the paper, the number of GCPs that can be used to satisfy the required accuracy is at least 5 points, but the optimal

number of GCPs to construct a high-accuracy DSM suitable for 1:1,000 scale mapping in mining projects is 20 points.

The results in Tables 3 and 4 show that not only does the number of GCPs affect the accuracy of DSM, but the location of these points also significantly influences the quality of the established model. The study selected GCPs at different locations such as: in the center, upper left corner, upper right corner, lower left corner, and

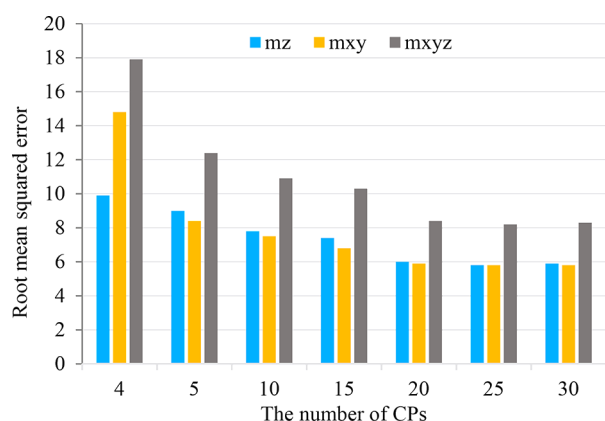


Fig. 8. Change in RMSE of GCPs with increasing GCPs

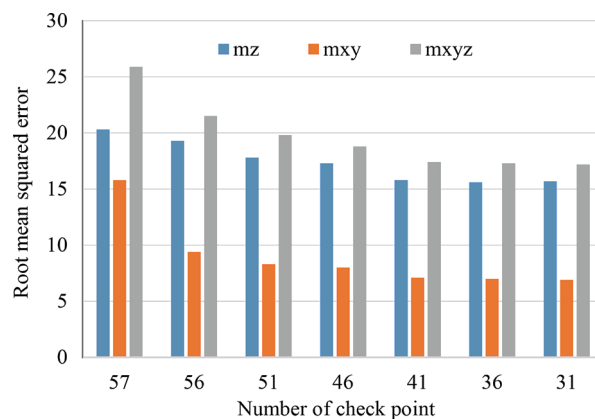


Fig. 9. Change in the RMSE of CPs with increasing GCPs

RMSEs of CPs for 7 cases

Number of GCPs	Cases	$RMSE_z$	$RMSE_{xy}$	$RMSE_{xyz}$	Number of GCPs	Cases	$RMSE_z$	$RMSE_{xy}$	$RMSE_{xyz}$
4	4_1	14.5	15.8	21.5	20	20_1	10.8	5.9	12.3
	4_2	23.9	16.3	28.9		20_2	17.4	8.7	19.6
	4_3	25.1	16.0	29.8		20_3	18.6	8.6	20.5
	4_4	24.7	16.1	29.5		20_4	22.1	7.2	23.3
	4_5	24.5	15.9	29.2		20_5	21.2	8.3	22.8
	4_6	17.3	16.2	23.8		20_6	14.9	6.7	16.3
	4_7	11.9	14.4	18.7		20_7	5.3	4.5	6.9
	Average	20.3	15.8	25.9		Average	15.8	7.1	17.4
5	5_1	15.2	8.9	17.6	25	25_1	11.2	5.8	12.6
	5_2	23.8	9.9	25.8		25_2	18.0	8.3	19.8
	5_3	23.0	9.7	24.9		25_3	18.4	8.2	20.2
	5_4	23.5	9.8	25.5		25_4	21.1	8.0	22.6
	5_5	23.3	9.6	25.2		25_5	20.8	7.8	22.2
	5_6	17.2	9.2	19.5		25_6	14.9	6.6	16.2
	5_7	8.8	8.4	12.2		25_7	5.1	4.4	6.7
	Average	19.3	9.4	21.5		Average	15.6	7.0	17.3
10	10_1	13.1	7.9	15.3	30	30_1	11.3	6.0	12.8
	10_2	23.2	8.6	24.8		30_2	17.6	8.0	19.4
	10_3	22.3	8.7	23.9		30_3	18.7	8.3	20.5
	10_4	22.5	8.6	24.1		30_4	21.5	7.1	22.7
	10_5	22.2	8.7	23.5		30_5	20.8	8.1	22.4
	10_6	16.5	8.4	18.6		30_6	14.7	6.5	16.1
	10_7	5.1	7.1	8.7		30_7	5.3	4.3	6.8
	Average	17.8	8.3	19.8		Average	15.7	6.9	17.2
15	15_1	12.1	7.8	14.4	—	—	—	—	—
	15_2	17.8	8.7	19.8	—	—	—	—	—
	15_3	21.9	8.5	23.5	—	—	—	—	—
	15_4	21.2	8.6	22.8	—	—	—	—	—
	15_5	21.5	8.5	23.1	—	—	—	—	—
	15_6	15.5	8.1	17.5	—	—	—	—	—
	15_7	11.3	6.3	10.5	—	—	—	—	—
	Average	17.3	8.0	18.8	—	—	—	—	—

lower right corner, evenly distributed, and at the edge of the measurement area as shown in Fig. 7. The selection of the location of these control points was applied to all 7 cases with the number of GCPs from 4 to 30. The results showed that, with any number of GCPs, the case where the selected points are concentrated at the corners of the study area has the largest error result (Figs. 10–12). The largest error is where only 4 control points are arranged in the upper left corner of the measuring area with an RMSE<sub>xy</sub> of 15.1 cm. With the points focusing on the lower left, upper right, and lower right corners, the RMSE<sub>xy</sub> are 14.8, 14.9, and 15.0 cm respectively. Since the points are concentrated at only one corner of the measurement area, the CPs in this case have a relatively large RMSE<sub>xy</sub> of 15.9–16.3 cm. Similarly, the altitude error of the GCPs in these cases is also up to 11.1–12.6 cm.

The accuracy can be increased if these points are distributed in the center. Compared with the case of GCPs arranged in the corner, the RMSE<sub>xy</sub> of GCPs has decreased from 0.3 to 0.9 cm. Specifically, from 15.1 to 14.2 cm (with 4 points), from 8.9 to 8.4 cm (with 5 points), from 7.9 to 7.4 cm (with 10 points), from 7.1 to 6.8 cm (with 15 points), from 6.4 to 6.0 cm (with 20, 25 points), from 6.4 to 5.9 cm (with 30 points). In addition, the error

of the CPs in these cases is reduced by 2 cm for the cases of 20 GCPs (from 8.7 to 6.7 cm), 25 GCPs (from 8.6 to 6.6 cm), and 30 GCPs (from 8.6 to 6.5 cm).

In addition, compared with the above 5 cases, the accuracy of the GCPs will be improved when they are placed at the edge of the measurement area. The RMSE<sub>xy</sub> of the GCPs can be decreased by 0.8 cm (for 5 GCPs), 0.7 cm (for 20, 25, 30 GCPs), and 0.5 cm (for 15 GCPs) in comparison to the case of points at the study area's corner. Similarly, the RMSE<sub>z</sub> of GCPs is reduced by 0.7–1.3 cm (case of 20, 25, 30 GCPs). In addition, the accuracy of GCPs in this case can be increased by 0.5 cm (25 GCPs) as compared to the points chosen in the center. For the control points, the distribution of GCPs at the edge of the study area also significantly improves their errors. The comparison results with RMSE of the case of GCPs distribution at the corner of the measurement area show that choosing the image control points at the edge of the measurement area helps the RMSE<sub>xy</sub> of the CPs to decrease up to 2.8 cm (20 points) while their height error can be reduced by the most to 11.3 cm (20 GCPs) and the least to 8.6 cm (5 GCPs).

The results in Tables 4 and 5 also show that, with any number of GCPs, the RMSE of both GCPs and CPs obtained is the smallest in the case where the GCPs are evenly distributed in the study area. In particular, the

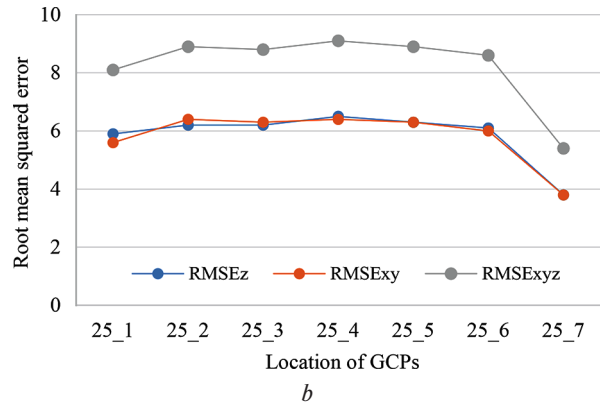
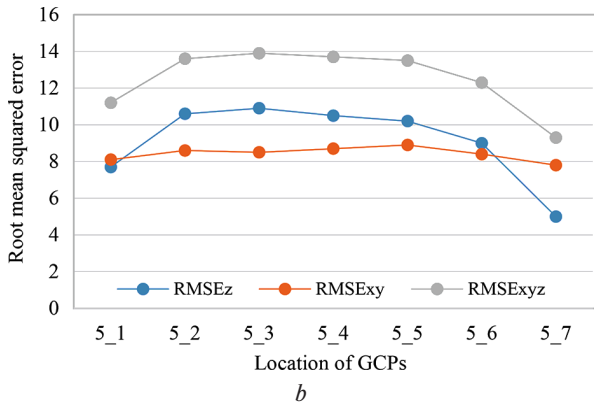
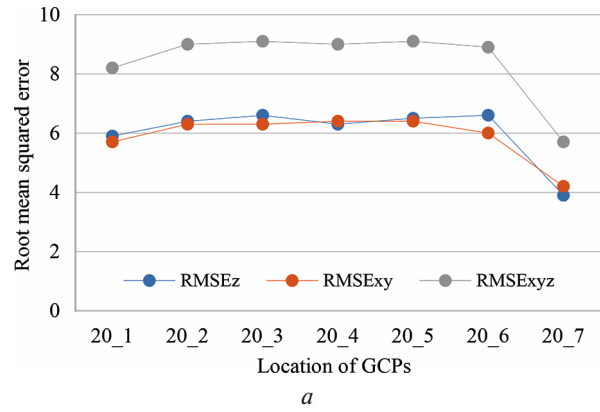
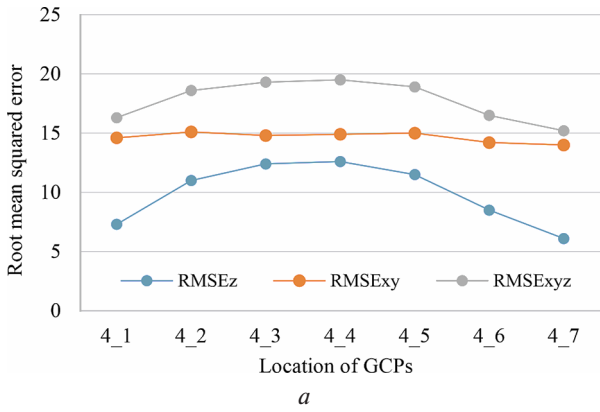


Fig. 10. Comparison of RMSE values for different numbers of GCPs:  
a – 4 GCPs; b – 5 GCPs

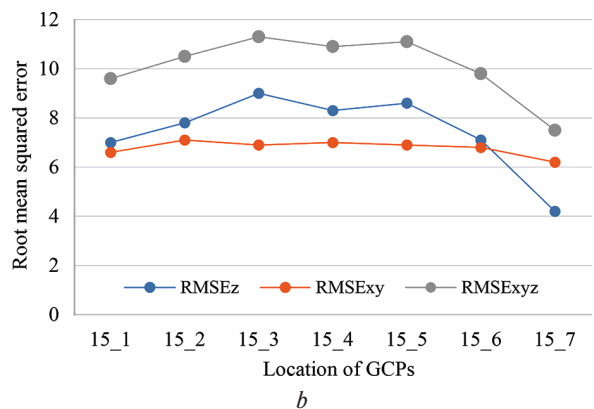
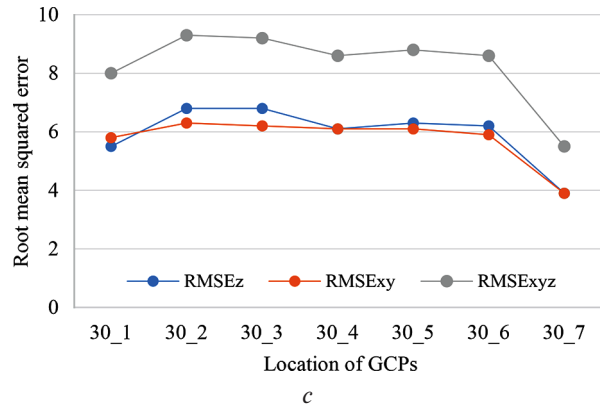
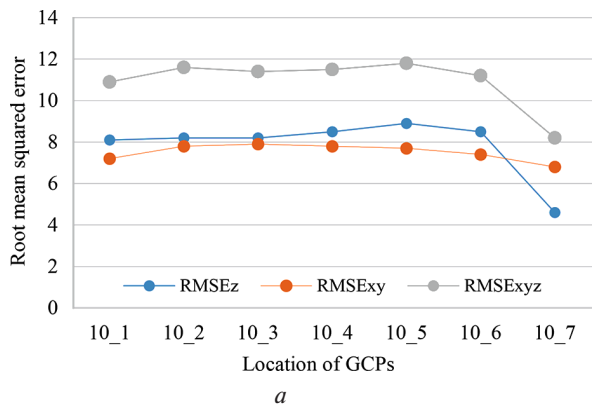


Fig. 12. Comparison of RMSE values obtained with (a) 4 GCPs and (b) 5 GCPs

Fig. 11. Comparison of RMSE values for different GCP configurations:  
a – 10 GCPs; b – 15 GCPs

RMSEz of GCPs decreased significantly compared to the case where these points were selected at the corner of the study area, specifically decreasing by 6.5 cm (4 GCPs), 5.9 cm (5 GCPs), 4.3 cm (10 GCPs), 5.8 cm (15 GCPs), 2.7 cm (20 GCPs), 3.1 cm (25 GCPs), 2.9 cm (30 GCPs). In the last three cases, due to the dense arrangement of GCPs, the accuracy of the elevation did not increase much compared to the other cases. In addition, the arrangement of GCPs evenly in the research region caused the RMSExy of GCPs to decrease from 1 to 2.5 cm. Accordingly, the accuracy of CPs in all cases also increased, increasing the most by 4.3 cm (30 GCPs) and increasing the least by 1.5 cm (5 GCPs).

The results obtained indicate that, to achieve both horizontal and vertical accuracy ensuring the precision of mapping at a scale of 1:1,000 in mining areas, the number of GCPs can be selected from 5 to 30 points. However, 20 GCPs are determined to be the optimal number for areas with the same area and terrain as the study area be-

cause this number of points gives the smallest RMSE<sub>xy</sub>, RMSE<sub>z</sub>, and RMSE<sub>xyz</sub> results. In addition, GCPs distributed evenly throughout the study area are recommended so that the DSM obtained has the highest accuracy.

**Limitations and future work.** A primary limitation of this study, as acknowledged in the background literature, is the focused exclusion of drone operational and camera parameters from the experimental analysis. While the study meticulously isolated the effect of GCPs, the final DSM accuracy remains intrinsically linked to flight conditions and settings that were held constant; however, the choice of these values directly dictates the Ground Sample Distance, which in turn limits the achievable geometric precision. Furthermore, the varied surface cover (bare rock, vegetation, stockpiles) inevitably introduces challenges related to image texture contrast and occlusion on steep slopes. These factors, along with potential variations in camera focal length or image quality due to weather, act as confounding variables that place an upper bound on the final DSM accuracy, regardless of the optimal GCP distribution. Future studies must systematically vary these flight and sensor parameters to fully decouple their individual influence from the geometric control provided by GCPs.

The empirical findings regarding the optimal deployment of 20 evenly distributed GCPs to achieve high-accuracy DSMs are highly relevant far beyond the mining industry, enhancing the generalizability of this research. In Land Management, the guidelines directly inform the establishment of precise topographic maps for cadastral surveying, urban planning, and volume change monitoring for regulatory purposes. For Environmental Monitoring, the ability to achieve consistent centimeter-level vertical accuracy is critical for reliably quantifying subtle changes, such as early-stage soil erosion, coastal dynamics, and ground subsidence. In Infrastructure Development, these principles ensure that construction projects including roads, pipelines, and large buildings are based on high-precision elevation data, minimizing errors in cut-and-fill estimates. Finally, Precision Farming can utilize these accurate DSMs to derive reliable topographical metrics like slope and aspect, essential for optimizing smart irrigation systems and managing within-field micro-topography variations to improve crop yield.

Moving forward, the research should be developed in several key directions to address the identified limitations and advance UAV photogrammetry practice. First, a dedicated investigation is needed to quantify the influence of flight altitude and image overlap variations on the resulting DSM RMSE across different terrain complexity levels. Second, it is crucial to evaluate the performance of Direct Georeferencing methods, specifically those leveraging high-accuracy Real-Time Kinematic or Post-Processed Kinematic systems onboard the UAV. Comparing the cost-effectiveness and accuracy of the optimal 20-GCP strategy against RTK/PPK flights with minimal or no GCPs will provide practical guidance for survey professionals seeking to further reduce fieldwork time and operational costs. Finally, the optimal configuration should be tested across a wider array of complex surface types such as areas with dense canopy, tall structures, or open water bodies to challenge the model's robustness and enhance the universal applicability of the proposed GCP deployment guidelines.

**Conclusion.** The study analyzed the influence of the number of image control points and their distribution on the accuracy of DSMs formed from UAV images. The results show that the number and distribution of GCPs have a significant impact on the precision of UAV-based DSMs. In addition, the study also revealed that the more control points, the higher the accuracy. However, depending on the area and terrain of the survey area, the number of GCPs should only increase to a certain limit.

For areas with small areas, characteristics, and complex terrain like the study area, 5 points are the minimum number of GCPs needed to ensure the accuracy of creating a 1:1,000 scale map. To reduce field survey work and ensure high accuracy, 20 GCPs are the optimal number for this study area. However, control points should be arranged evenly in the survey area to achieve the highest accuracy.

The research offers valuable insights for professionals utilizing UAV technology in topographic mapping and resource management. It emphasizes the critical role of carefully planning both the quantity and spatial distribution of ground control points to achieve high-accuracy digital surface models. These guidelines help optimize field survey efforts and reduce operational costs without compromising data quality. The findings are especially relevant for surveying areas with complex terrain, supporting decision-making in mining, land management, environmental monitoring, infrastructure development, and precision agriculture. By applying the principles identified in this study, practitioners can ensure more reliable mapping outcomes, improve project efficiency, and contribute to better management of natural and built environments.

**Acknowledgments.** Thanks to anonymous reviewers and editorial comments for their valuable comments in the earlier version, which helped us to improve the manuscript's quality.

#### References.

1. Minh, D. T., & Dung, N. B. (2023). Applications of UAVs in mine industry: A scoping review. *Journal of Sustainable Mining*, 22(2), 128-145. <https://doi.org/10.46873/2300-3960.1384>
2. Kaushal, H., & Bhatnagar, H. (2022). Application of Drones in Mining industry-rules, guidelines and case study. *Journal of emerging technologies and innovative research*, 12, 459-470.
3. Bhandari, B., Oli, U., Pudasaini, U., & Panta, N. (2015). Generation of high resolution DSM using UAV images. *FIG working week*, 17-21. Retrieved from <https://www.researchgate.net/publication/311650666>
4. Puniach, E., Gruszczynski, W., Cwiakala, P., & Matwij, W. (2021). Application of UAV-based orthomosaics for determination of horizontal displacement caused by underground mining. *ISPRS Journal of Photogrammetry and Remote Sensing*, 174, 282-303. <https://doi.org/10.1016/j.isprsjprs.2021.02.006>
5. Vemulapalli, S. C., & Mesapam, S. (2021). Slope stability analysis for mine hazard assessment using uav. *Journal of the Indian Society of Remote Sensing*, 49, 1483-1491. <https://doi.org/10.1007/s12524-020-01239-9>
6. Carabassa, V., Montero, P., Alcañiz, J. M., & Padró, J.-C. (2021). Soil erosion monitoring in quarry restoration using drones. *Minerals*, 11(9), 949. <https://doi.org/10.3390/min11090949>
7. Nguyen, B. D. (2023). Identifying the Potential Application of Unmanned Aerial Vehicle Technology in Mine Waste Dumps. *Inżynieria Mineralna*, 52(2). <http://doi.org/10.2922/IM-2023-02-2>
8. Baltiyeva, A., Orynassarova, E., Zharaspaev, M., & Akhmetov, R. (2023). Studying sinkholes of the earth's surface involving radar satellite interferometry in terms of Zhezkazgan field, Kazakhstan. *Mining of Mineral Deposits*, 17(4), 61-74. <https://doi.org/10.33271/mining17.04.061>
9. Gehrke, S., Morin, K., Downey, M., Boehrer, N., & Fuchs, T. (2010). Semi-global matching: An alternative to LIDAR for DSM generation. *Proceedings of the 2010 Canadian Geomatics Conference and Symposium of Commission I*, 2(6), 1-6. Retrieved from [https://www.isprs.org/proceedings/XXXVIII/part1/11/11\\_01\\_Paper\\_121.pdf](https://www.isprs.org/proceedings/XXXVIII/part1/11/11_01_Paper_121.pdf)

10. Lastilla, L., Belloni, V., Ravanelli, R., & Crespi, M. J. R. S. (2021). DSM generation from single and cross-sensor multi-view satellite images using the new agisoft metashape: The case studies of Trento and Matera (Italy). *Remote Sensing*, 13(4), 593. <https://doi.org/10.3390/rs13040593>

11. Hwang, J. T., Chen, Y. W., Lian, W. Y., Yang, Y. Y., & Chu, T. C. (2015). DSM generation on the shade of tree area of aerial photogrammetry. 2015 23<sup>rd</sup> International Conference on Geoinformatics, 1-4. <https://doi.org/10.1109/GEOINFORMATICS.2015.7378601>

12. Ulvi, A. (2021). The effect of the distribution and numbers of ground control points on the precision of producing orthophoto maps with an unmanned aerial vehicle. *Journal of Asian Architecture and Building Engineering*, 20(6), 806-817. <https://doi.org/10.1080/13467581.2021.1973479>

13. Ulvi, A. (2018). Analysis of the utility of the unmanned aerial vehicle (UAV) in volume calculation by using photogrammetric techniques. *International journal of engineering and geosciences*, 3(2), 43-49. <https://doi.org/10.26833/ijeg.377080>

14. Nguyen, L. Q. (2021). Accuracy assessment of open-pit mine's digital surface models generated using photos captured by Unmanned Aerial Vehicles in the post-processing kinematic mode. *Journal of Mining and Earth Sciences*, 62(4), 38-47. [https://doi.org/10.46326/JMES.2021.62\(4\).05](https://doi.org/10.46326/JMES.2021.62(4).05)

15. Clapuyt, F., Vanacker, V., & Van Oost, K. (2016). Reproducibility of UAV-based earth topography reconstructions based on Structure-from-Motion algorithms. *Geomorphology*, 260, 4-15. <https://doi.org/10.1016/j.geomorph.2015.05.011>

16. Rock, G., Ries, J., & Udelhoven, T. (2012). Sensitivity analysis of UAV-photogrammetry for creating digital elevation models (DEM). *The International Archives of the Photogrammetry, Remote Sensing and Spatial Information Sciences*, 38, 69-73. <https://doi.org/10.5194/isprsarchives-XXXVIII-1-C22-69-2011>

17. Nouwakpo, S. K., Weltz, M. A., & McGwire, K. (2016). Assessing the performance of structure-from-motion photogrammetry and terrestrial LiDAR for reconstructing soil surface microtopography of naturally vegetated plots. *Earth Surface Processes and Landforms*, 41(3), 308-322. <https://doi.org/10.1002/esp.3787>

18. Oniga, V.-E., Breaban, A.-I., Pfeifer, N., & Chirila, C. (2020). Determining the suitable number of ground control points for UAS images georeferencing by varying number and spatial distribution. *Remote Sensing*, 12(5), 876. <https://doi.org/10.3390/rs12050876>

19. Martínez-Carricondo, P., Agüera-Vega, F., Carvajal-Ramírez, F., Mesas-Carrascosa, F. J., García-Ferrer, A., & Pérez-Porrás, F. J. (2018). Assessment of UAV-photogrammetric mapping accuracy based on variation of ground control points. *International journal of applied earth observation and geoinformation*, 72, 1-10. <https://doi.org/10.1016/j.jag.2018.05.015>

20. Sanz-Ablanedo, E., Chandler, J. H., Rodríguez-Pérez, J. R., & Ordóñez, C. (2018). Accuracy of unmanned aerial vehicle (UAV) and SfM photogrammetry survey as a function of the number and location of ground control points used. *Remote Sensing*, 10(10), 1606. <https://doi.org/10.3390/rs10101606>

21. Gomes Pessoa, G., Caceres Carrilho, A., Takahashi Miyoshi, G., Amorim, A., & Galo, M. (2021). Assessment of UAV-based digital surface model and the effects of quantity and distribution of ground control points. *International Journal of Remote Sensing*, 42(1), 65-83. <https://doi.org/10.1080/01431161.2020.1800122>

22. Agüera-Vega, F., Carvajal-Ramírez, F., & Martínez-Carricondo, P. (2017). Assessment of photogrammetric mapping accuracy based on variation ground control points number using unmanned aerial vehicle. *Measurement*, 98, 221-227. <https://doi.org/10.1016/j.measurement.2016.12.002>

23. Long, N. Q., Goyal, R., Bui, L. K., Cuong, C. X., Canh, L. V., Minh, N. Q., & Bui, X. N. (2021). Optimal choice of the number of ground control points for developing precise DSM using light-weight UAV in small and medium-sized open-pit mine. *Archives of Mining Sciences*, 66(3), 369-384. <https://doi.org/10.24425/ams.2021.138594>

24. Rangel, J. M. G., Gonçalves, G. R., & Pérez, J. A. (2018). The impact of number and spatial distribution of GCPs on the positional accuracy of geospatial products derived from low-cost UASs. *International Journal of Remote Sensing*, 39(21), 7154-7171. <https://doi.org/10.13140/RG.2.2.29670.52807>

25. Villanueva, J. K. S., & Blanco, A. C. (2019). Optimization of ground control point (GCP) configuration for unmanned aerial vehicle (UAV) survey using structure from motion (SfM). *The international archives of the photogrammetry, remote sensing and spatial information sciences*, 42, 167-174. <https://doi.org/10.5194/isprs-archives-XLII-4-W12-167-2019>

26. Shahbazi, M., Sohn, G., Théau, J., & Menard, P. (2015). Development and evaluation of a UAV-photogrammetry system for precise

3D environmental modeling. *Sensors*, 15(11), 27493-27524. <https://doi.org/10.3390/s151127493>

27. Nguyen, Q. L., Bui, X. N., Cao, X. C., & Le, V. C. (2019). An approach of mapping quarries in Vietnam using low-cost Unmanned Aerial Vehicles. *Inżynieria Mineralna*, 21. <https://doi.org/10.29227/IM2025-n-1-v1>

28. Tonkin, T. N., & Midgley, N. G. (2016). Ground-control networks for image based surface reconstruction: An investigation of optimum survey designs using UAV derived imagery and structure-from-motion photogrammetry. *Remote Sensing*, 8(9), 786. <https://doi.org/10.3390/rs8090786>

29. Long, N. Q. (2021). Research proposes a process of establishing large scale topographic maps 1:2,000, 1:1,000 and 1:500 for the topographic of open pit mine area in vietnam using low-cost uavs and common cameras. *Ministerial-level scientific research project*.

## Опорні пункти та їхній вплив на точність створення цифрової моделі поверхні за допомогою безпілотного літального апарату

Ань Туан Луу\*

Ханойський університет гірничої справи та геології, факультет геоматики та управління земельними ресурсами, м. Ханой, Соціалістична Республіка В'єтнам

\* Автор-кореспондент e-mail: [luuanhtuan@humg.edu.vn](mailto:luuanhtuan@humg.edu.vn)

**Мета.** Визначення оптимальної кількості й просторового розташування опорних пунктів (GCPs), необхідних для досягнення високої точності геоприв'язки зображень, отриманих із безпілотного літального апарату (БПЛА), зокрема для картографування у масштабі 1:1 000.

**Методика.** Створені сім експериментальних сценаріїв, у яких кількість опорних пунктів варіювалася від 4 до 30. Для кожного сценарію опорні пункти розміщувалися за сімома різними схемами: у центрі, по кутах, по краях і рівномірно по площі. Для оцінки точності геоприв'язки для кожної конфігурації розраховувалося середньоквадратичне відхилення (RMSE).

**Результати.** Встановлено, що використання лише 4 опорних пунктів призводить до найвищого значення RMSE, тобто найнижчої точності. Значення RMSE зменшуються зі збільшенням кількості опорних пунктів, проте покращення після 20 пунктів є незначним. Серед усіх варіантів розташування найвищі значення RMSE спостерігалися при розміщенні опорних пунктів по кутах. Найточніші результати отримані при рівномірному розташуванні 20 опорних пунктів.

**Наукова новизна.** У роботі вперше здійснена системна оцінка як кількості, так і просторового розміщення опорних пунктів у фотограмметрії із використанням БПЛА, що надає емпіричне обґрунтування оптимальних стратегій їх розташування.

**Практична значимість.** Отримані результати мають практичну цінність для фахівців у сфері картографування за допомогою БПЛА, адже свідчать, що для досягнення точності, необхідної для карт масштабу 1:1 000, достатньо використання 20 рівномірно розміщених опорних пунктів. Це дозволяє підвищити ефективність польових робіт і забезпечити високу якість даних.

**Ключові слова:** опорні пункти, цифрова модель поверхні, безпілотний літальний апарат

*The manuscript was submitted 06.09.25.*